Accepted Manuscript

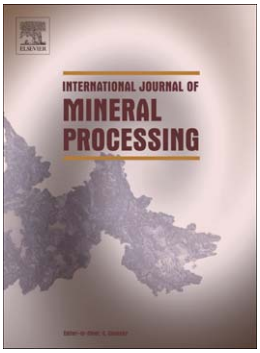

The interaction between copper species and pyrite surfaces in copper cyanide solutions

Bao Guo, Yongjun Peng

PII: S0301-7516(16)30254-X
DOI: doi: 10.1016/j.minpro.2016.11.021
Reference: MINPRO 2993

To appear in: *International Journal of Mineral Processing*

Received date: 11 May 2016
Revised date: 17 November 2016
Accepted date: 23 November 2016

Please cite this article as: Guo, Bao, Peng, Yongjun, The interaction between copper species and pyrite surfaces in copper cyanide solutions, *International Journal of Mineral Processing* (2016), doi: 10.1016/j.minpro.2016.11.021

The interaction between copper species and pyrite surfaces in copper cyanide solutions

*Bao Guo and Yongjun Peng**

School of Chemical Engineering, the University of Queensland, St. Lucia, Brisbane, QLD 4072, Australia.

*Corresponding author. Tel: +61 7 336 57156. Email address: yongjun.peng@uq.edu.au

Abstract: The adsorption of copper ions and the formation of a copper sulfide phase on pyrite surfaces are of vital importance to alter the surface property of pyrite and determine its fate either to be rejected in the flotation of polymetallic sulfide ores or to be recovered in the flotation of pyritic gold ores. Cyanide and copper may co-exist in the process water with complicated speciation. The objective of this study is to understand the interaction between copper cyanide species and pyrite and clarify the possible adsorption of copper on pyrite surfaces from cyanide-bearing solutions. Surface-enhanced Raman spectroscopy and electrochemical measurements were used to determine the reaction products formed on pyrite surfaces. It was found that Cu(I)-bearing species were incorporated into pyrite, forming a CuS-like sulfide from copper cyanide solutions at a more oxidizing potential, while a Cu_2S-like sulfide formed at a more reducing potential. The amount of copper deposited on pyrite was significantly improved at a more reducing potential at which the pyrite surface tended to be FeS-like. In addition, these Cu(I)-sulfides on pyrite surfaces were dissolved by cyanide-bearing species at a high CN/Cu ratio, compromising the total amount of copper uptake.

Keywords**:** Pyrite; Copper cyanide; Copper adsorption; Redox products; Flotation

1. Introduction

Pyrite responds well to thiol collectors such as xanthates and its flotation presents two maximums at around pH 4 and 8 with a depression at around pH 7 (Fuerstenau et al., 2007; Wang et al., 1989a). The high flotation yield at pH 4 is due to the formation of sulfur-rich products and dixanthogen (Leppinen, 1990; López Valdivieso et al., 2005). The yield at pH 8 is due to the formation of iron hydroxide-xanthate complexes on pyrite surfaces (Fornasiero and Ralston, 1992). The depression at around pH 7 is due to a high density of ferric hydroxides on pyrite surfaces, which, however, disappear with the increase of xanthate concentration due to the reduction of ferric hydroxides to ferrous species resulting from the oxidation of xanthate to dixanthogen (López Valdivieso et al., 2005). The depression above pH 11 is due to the thermodynamic instability of dixanthogen and the formation of ferric hydroxide islands on pyrite surfaces (Leppinen, 1990; Fuerstenau et al., 2007).

Cu^{2+} can activate pyrite and then enhance the adsorption of xanthate resulting in good floatability at neutral to alkaline pH (Chandra and Gerson, 2009; Finkelstein, 1997; Laajalehto, 1999; Leppinen, 1990; Weisener and Gerson, 2000a; Weisener and Gerson, 2000b; Wang et al., 1989b). The copper activation process on pyrite surfaces has been considered to be an electrochemical process involving the adsorption of Cu^{2+} onto pyrite surfaces and the reduction of Cu(II) to Cu(I) with simultaneous oxidation of pyrite resulting in the formation of a Cu(I)-sulfide phase (Weisener and Gerson, 2000a; Weisener and Gerson, 2000b). The adsorption of Cu^{2+} on pyrite is more favorable in reducing conditions (Chen, 1998). Cu^{2+} dissolved from copper minerals such as chalcopyrite and chalcocite through a galvanic interaction may activate pyrite inadvertently and deteriorate the separation of copper and other base metal sulphide minerals from pyrite in flotation (Peng et al., 2003). To ensure the selectivity between pyrite and

other base metal sulphides in the presence of copper ions, the deactivation of copper ions on pyrite surfaces will be required.

Cyanide is added intentionally to depress pyrite or deactivate copper activation on pyrite surfaces in the flotation of copper, lead and zinc ores. The mechanism of pyrite-cyanide interactions has been generally accepted as cyanide preferentially adsorbing on pyrite with iron cyanide compounds inhibiting electrochemical activities on the surface (Elgillani and Fuerstenau, 1968; Janetski et al., 1977; Wang and Forssberg, 1996). Copper and cyanide co-existing in solution show complicated speciation, depending on the pH and cyanide-to-copper ratio (Dai et al., 2012; Lu et al., 2002; Lukey et al., 1999). Cuprous tetra-cyanide ($Cu(CN)_4^{3-}$), cuprous tri-cyanide ($Cu(CN)_3^{2-}$), and cuprous di-cyanide ($Cu(CN)_2^{-}$) are the most common cuprous cyanide species. Cuprous cyanide species are also present in the process water from gold cyanidation recycled to flotation circuits and may inadvertently affect the flotation of pyrite where precious metals are always associated with (Adams, 2013).

Practical operations have demonstrated that pyrite can be activated on the one hand but depressed on the other hand in copper and cyanide-bearing environments. $Cu(CN)_3^{2-}$ was found to depress pyrite in the flotation of pyritic gold ores at pH 10 (Guo et al., 2015). However, the impact of cuprous cyanide on mineral flotation is rather complicated. Cuprous cyanide was found to activate mineral flotation as well (Prestidge et al., 1997; Seke and Pistorius, 2006). A distinctive aspect of pyrite is the occurrence of variable surface compositions subjecting to oxidizing or reducing aqueous solutions (Murphy and Strongin, 2009). Pyrite surfaces after fracturing show both S monomers (S(–II)) and S-S dimers ($S(-I)_2$) (Von Oertzena et al., 2006). The intermediate oxidation of pyrite leads to the formation of ferric hydroxides and a sulfur-rich layer (elemental sulfur (S^0), poly-sulfides (FeS_n) or metal-deficient sulfide ($Fe_{1-x}S_2$)) (Buckley

and Woods, 1987; Hamilton and Woods, 1981; Yoon et al., 1991). The extensive oxidation of pyrite to sulfate occurs at more positive potentials while the reductive decomposition of pyrite to a FeS-like surface with dominant S monomers takes place at more negative potentials (Hamilton and Woods, 1981; Tao et al., 2003). The competitive adsorption between copper and cyanide may also change pyrite surface chemistry.

In this study, the adsorption of copper ions on pyrite surfaces from cyanide-bearing solutions was investigated via an electrochemical approach including voltammetry and impedance measurements by taking into account the redox potential and cyanide-to-copper ratio. The reaction products were determined by surface-enhanced Raman spectroscopy and the surface reactions taking place on pyrite surfaces were discussed from a thermodynamic aspect. This study suggests the chemical conditions for the activation and deactivation of copper ions on pyrite surfaces in copper and cyanide-bearing environments, which is valuable for the selective flotation of other base metal sulfide minerals against pyrite and also for the flotation of pyritic gold ores where gold is recovered with pyrite.

2. Experimental methods

2.1. Materials

Copper cyanide solutions were prepared by dissolving copper(I) cyanide powder (CuCN, 99.99%, Aldrich) to sodium cyanide (NaCN, 99.9%, Aldrich) solutions to give the final solutions with CN/Cu=2/1, 2.5/1, 3/1, 3.5/1 and 4/1. A hand-picked natural massive cubic pyrite specimen originating from Spain was used as the working electrode. Energy Dispersive Spectroscopy (EDS) analysis on the pyrite specimen showed 66.35 at.% sulfur and 33.17 at.% iron with minor carbon contamination. XRD analysis also showed a high purity of the pyrite specimen with minor quartz and galena minerals.

2.2. Electrochemical Measurements

The pyrite electrode was connected with a copper wire using a silver-loaded conducting epoxy, and then mounted into non-conducting epoxy resin exposing only one side with a geometric surface of approximately 0.25 cm^2. A platinum plate with a surface area of 1 cm^2 was utilized as the auxiliary electrode (counter electrode). Potentials were measured and reported against an Ag/AgCl reference electrode filled with 3 M KCl which has a potential of +0.1915 V against the standard hydrogen electrode (SHE). A Radiometer PGZ100 potentiostat was used in combination with a frequency response analyzer (FRA).

A fresh electrode surface was generated before each experimental run by wet abrading with silicon carbide abrasive paper (1200 grits). The previous study on Cu^{2+} activation confirmed that the oxidation of pyrite during polishing did not have a strong influence on copper adsorption and similar results were obtained between the polished and in-situ fractured pyrite electrodes (Chen, 1998). A pretreatment of the pyrite electrode was conducted at a certain polarization potential in a deoxygenated solution containing copper cyanide at pH 7 for 10 min under stirring (50 rpm/m). The copper cyanide solution was then removed from the electrochemical cell which was then filled with a deoxygenated solution without copper ions for electrochemical measurements. Nitrogen gas was applied above the solution to expel the return of oxygen. The measurement system (electrochemical cell) was sealed to minimize the volatilization of HCN from aqueous phase to gas phase during the experiment. For a closed and static system, less than 0.05% of the total aqueous HCN volatilizes (Lotter, 2006). The actual volatilized HCN during mineral processing should be evaluated and monitored before any large scale application.

Cyclic voltammetry (CV) and Electrochemical Impedance Spectroscopy (EIS) measurements were performed in a 0.2 L background solution with 0.1 M potassium dihydrogen phosphate

(KH_2PO_4, 99.9%, Aldrich) at room temperature. The pH was adjusted to 7 with a KOH solution. All solutions were prepared with deionized water. The potential scan rate for CV was 0.02 V s^{-1}. EIS was conducted at a DC applied potential of 0.1 V which was close to the open circuit potential of pyrite, and at an AC potential of 0.01 V. Typically, the electrode surface was stabilized at the desired DC potential for 5 min after which EIS was obtained.

2.3. Raman Spectroscopy Measurements

Raman spectroscopy measurements were conducted with a Renishaw Raman spectrometer using 632.8 nm red excitation from a He-Ne laser. The scattered light was detected with a CCD detector cooled to −50°C with the spectral resolution of 2.7 cm^{-1}. The laser and scattered radiation were focused through the spectrometer objective lenses with a long working distance. The laser spot size was ~1.3 μm and the laser power at the sample was 0.6 mW (10% power). Spectra were collected for 10 seconds with 20 accumulations. The grating was calibrated using the 520 cm^{-1} silicon band. Surface enhancement was achieved by sputtering fine gold (99.5% Au) on pyrite surfaces using K550X sputter coater. The specimen was placed in a chamber which was then evacuated to a vacuum of 10^{-4} mbar. Gold was sputtered for 2 min at a coating current of 25 mA from a target located 60 mm away from and 4 cm above the sample. The gold-coated pyrite electrode was pre-treated at a certain polarization potential in a deoxygenated solution containing copper cyanide at pH 7 for 10 min under stirring at 50 rpm/m, and then transferred to the spectrometer chamber for measurements under nitrogen protection.

3. Results

This research started with understanding the copper adsorption on pyrite surfaces in the copper cyanide solution with CN/Cu=2/1 at different polarization potentials. The reaction taking place on pyrite surfaces were studied by cyclic voltammetry, the reaction products formed were

determined by surface-enhanced Raman spectroscopy and the properties of the surface layer structure as a result of copper adsorption was analyzed by electrochemical impedance spectroscopy. Then how Cn/Cu ratios affected the copper adsorption on pyrite surfaces was investigated.

3.1. Copper Adsorption on Pyrite Surfaces at CN/Cu=2/1

Cyclic voltammetry

The voltammogram of the untreated pyrite electrode exposing to the background solution at pH 7 is shown in Fig. 1(a). The anodic peak A1 commencing at −0.27 V is due to the intermediate oxidation of pyrite through Equation (1), (2) or (3) (Buckley and Woods, 1987; Hamilton and Woods, 1981; Yoon et al., 1991).

$$FeS_2 + 3H_2O \rightarrow Fe(OH)_3 + 2S^0 + 3H^+ + 3e^- \quad (1)$$

$$nFeS_2 + 3(n-2)OH^- \rightarrow 2FeS_n + (n-2)Fe(OH)_3 + 3(n-2)e^- \quad (2)$$

$$FeS_2 + 3xOH^- \rightarrow xFe(OH)_3 + Fe_{1-x}S_2 + 3xe^- \quad (3)$$

The extensive oxidation of pyrite as shown in Equation (4) occurs at peak A2 at an elevated potential, leading to a steady increase in current with increasing the potential (Buckley and Woods, 1987; Hamilton and Woods, 1981; Yoon et al., 1991).

$$FeS_2 + 11H_2O \rightarrow Fe(OH)_3 + 2SO_4^{2-} + 19H^+ + 15e^- \quad (4)$$

A cathodic peak C1 at −0.35 V with a current shoulder C1′ at around −0.1 V arises from the reduction of oxidation products formed during the prior anodic scan. The possible reduction process can be represented by Equation (5) with the formation of a FeS-like product (Tao et al., 2003). The variation of *n* values leads to a broad range from C1′ to C1 for occurrence of the reduction reaction.

$$FeS_n + (n-1)Fe(OH)_3 + 3(n-1)e^- \rightarrow nFeS + 3(n-1)OH^- \quad (5)$$

Some researchers disagreed with Equation (5) and proposed a product similar to pyrite after reduction (Velásquez et al., 2005). The cathodic peak C1 also contains a contribution from the reduction of ferric hydroxide to ferrous hydroxide with a much higher solubility in neutral media (Tao et al., 2003). Peak C1 may be attributed to the reduction of S^0 to HS^- as well. Hydrogen sulfide (H_2S), as the conjugate base of HS^-, also forms at neutral pH. Both HS^- and H_2S are soluble in the solution. The reductive decomposition of pyrite takes place at more negative potentials (Hamilton and Woods, 1981; Tao et al., 2003), resulting in a further decrease in current with decreasing the potential at peak C2. The reaction can be presented by:

$$FeS_2 + H_2O + 2e^- \rightarrow FeS + HS^- + OH^- \quad (6)$$

Figure 1(b) shows the voltammograms of the pyrite electrode pretreated in the copper cyanide solution with CN/Cu=2/1 at 0 V, −0.2 V, −0.4 V and −0.6 V. The voltammograms were initiated from 0.1 V which was around the open circuit potential of pyrite to 0.4 V on an anodic scan, and then switched to −0.6 V on a cathodic scan. Fig. 1(b) only shows the second cycle of voltammograms. Compared to the voltammogram of the untreated pyrite electrode, an additional peak A3 arises on the anodic scan and an additional peak C3 arises on the cathodic scan for the pyrite electrode pretreated in the copper cyanide solution with CN/Cu=2/1 at all potentials. Peaks A3 and C3 may be due to the adsorption of copper species on pyrite surfaces.

A number of researchers have studied pyrite activation by Cu^{2+} in the absence of cyanide species. Using Fourier Transform Infrared Spectroscopy (FTIR), it was proposed that the surface species formed on pyrite activated by Cu^{2+} resembled chalcocite (Cu_2S) rather than covellite (CuS) based on the FTIR spectrum of adsorbed xanthate which closely resembled that of copper(I) xanthate (Leppinen 1990). Chen (1998) observed the oxidation of Cu_2S on the

voltammogram of Cu^{2+}-activated pyrite. Chalcocite (Cu_2S) can be oxidized through Equation (7) (Chen and Yoon, 2000; Velásquez et al., 2001).

$$Cu_2S + xH_2O \rightarrow xCuO + Cu_{2-x}S + 2xH^+ + 2xe^- \quad (7)$$

According to the *Eh*-pH diagram of copper sulfide species (Woods et al., 1987), reaction (7) occurs at potentials in the range of approximately 0.25 to 0.45 V (SHE) which is consistent with the potential at which peak A3 appears in Fig. 1(b). On the cathodic scan, a well-defined peak C3 occurs and should be attributed to the reverse of Equation (7). It seems that pyrite is activated by the copper cyanide solution with CN/Cu=2/1 when treated at 0 V, −0.2 V, −0.4 V or −0.6 V, corresponding to a Cu(I)-sulfide phase formed on the surface.

Figure 1(b) also shows that the current densities at A3 and C3 are very small with little change at the polarization potential varying from 0 V to −0.2 V, but increase with the polarization potential decreasing to −0.6 V. On the other hand, the oxidation and reduction reactions at A1 and C1/C1′ due to pyrite oxidation and reduction are both inhibited especially at more negative polarization potentials. This suggests that the formation of Cu(I)-sulfide on pyrite surfaces causes passivation of pyrite surfaces, restricting further surface oxidation.

Surface-Enhanced Raman Spectroscopy

Recently, surface-enhanced Raman scattering (SERS) techniques have been developed to identify species formed on mineral surfaces which were coated with a sputtered film of gold (Hope et al., 2007). In this study, surface-enhanced Raman spectroscopy was used to characterize the reaction products formed on pyrite surfaces in copper cyanide solutions. The obtained Raman spectra for the untreated pyrite electrode and the pyrite electrode pretreated in the copper cyanide solution with CN/Cu=2/1 at 0 V, −0.2 V, −0.4 V and −0.6 V are shown in Fig. 2. From literature, the cubic cell of FeS_2 crystal consists of Fe atoms and S_2 units that form

interpenetrating Face-Centered Cubic (FCC) lattice, and the sulfur dimers lie in the [111] directions (Mernagh and Trudu, 1993). The Raman spectra of pyrite show two peaks at 340 cm^{-1} and 380 cm^{-1} with the lower energy shift due to the S displacement perpendicular to the sulfur dimer direction and the higher energy shift due to the stretching vibration of S_2 throughout the crystal. A small feature at 430 cm^{-1} is due to lattice modes (Hope et al., 2001; Turcotte et al., 1993). Those Raman bands are all identified on the pyrite coated with gold in the present study (Fig. 2). The gold-cyanide stretching displays a band at 382 cm^{-1}, 295 cm^{-1}, and 2126 cm^{-1} (Beltramo et al., 2004; Pettinger et al., 2003). Since the Raman spectra in Fig. 2 do not show any assignment for gold-bearing species, the gold coating on pyrite may not have an influence on the surface speciation of pyrite interacting with copper cyanide.

The Raman spectra of copper sulfides have also been reported previously. The Raman spectra of covellite consist of an S-S stretch at 474 cm^{-1} and a small peak at 267 cm^{-1} (Ishii et al., 1993). The Raman spectra of chalcocite (Cu_2S) display a broad weak band at around 300 cm^{-1} and a small peak at 225 cm^{-1}, and they are only visible when the laser intensity is low (Parker et al., 2003). A range of stable and metastable copper sulfides has been identified with the stoichiometry between those of chalcocite and covellite (Turcotte et al., 1993). In the present study, the Raman spectra of the pyrite electrode pretreated in the copper cyanide solution with CN/Cu=2/1 at −0.6 V and −0.4 V exhibited distinct stretching bands at 225 cm^{-1} and 300 cm^{-1} resulting from the formation of Cu_2S. The formation of CuS existed on the pyrite electrode pretreated in the copper cyanide solution at −0.2 V and 0 V due to distinct stretching bands at 475 cm^{-1}. There is also a weak broad stretching band at about 300 cm^{-1} on the Raman spectra of the pyrite electrode pretreated at 0 V and −0.2 V, indicating the formation of a small amount of Cu_2S as well.

The Raman spectra in Fig.2 show that both Cu_2S and CuS can form on pyrite surfaces in the copper cyanide solution with CN/Cu=2/1 depending on the polarization potential. In addition to the oxidation of Cu_2S in Equation (7) which explains the appearance of peak A3 in Fig. 1(b), peak A3 in Fig. 1(b) can also result from the oxidation of CuS to non-stoichiometric copper sulfides as follows (Woods et al., 1987):

$$n\mathrm{CuS}+(n-1)\mathrm{H_2O}\rightarrow(n-1)\mathrm{CuO}+\mathrm{CuS}_n+2(n-1)\mathrm{H^+}+2(n-1)\mathrm{e^-} \quad (8)$$

In fact, CuS can be converted to Cu_2S through Equation (9) (Chen and Yoon, 2000).

$$2\mathrm{CuS}+\mathrm{H^+}+2\mathrm{e^-}\rightarrow\mathrm{Cu_2S}+2\mathrm{HS^-} \quad (9)$$

Electrochemical Impedance Spectroscopy

The surface layer structure as a result of copper adsorption on pyrite was analysed by EIS. The analysis of impedance spectra relies on the modelling of an electrical equivalent circuit with physical elements. In this study, based on the criteria of simplicity and electrochemical interpretation, the electrical circuit shown in Fig. 3 was used to model the electrochemical process at the mineral/solution interface. In this electrical circuit, R_s is the solution resistance and other Ohmic resistances which show little change for all the tests, C_{dl} is the double-layer capacitance, R_{ct} is the charge transfer resistance, Q_{sl} is the surface layer capacitance which can be present as either the initial pyrite oxidation species or the formed copper species, and R_p is the pore resistance of the layer.

A capacitor forms when two conducting plates are separated by a non-conducting medium which is also called dielectric with its impedance being $-j/\omega C$ where ω is the angular frequency of the AC voltage. The value of the capacitance C can be described as Equation (10).

$$C=\varepsilon_0\varepsilon_r A/d \quad (10)$$

where ε_0 is the permittivity of free space which is a physical constant, d is the distance between two plates, A is the surface area of the plate, and ε_r is the dielectric constant which varies with material. Q_{sl} was modelled by a constant phase element (CPE) in place of an ideal capacitor with its impedance defined in Equation (11).

$$Z = \frac{1}{Y_0(j\omega)^n} \quad (11)$$

where Y_0 is the CPE constant, and n is the CPE power. CPE is a useful modelling parameter governed by the physical nature of electrodes and surface reactions such as surface roughness, "leaky" capacitor and non-uniform current distribution.

Figure 4 presents the Bode plots of the pyrite electrode pretreated in the copper cyanide solution with CN/Cu=2/1 at 0 V, −0.2 V, −0.4 V and −0.6 V. The Bode plots were plotted with log frequency on the X-axis and both the absolute values of impedance Z (Fig. 4(a)) and the phase-shift (Fig. 4(b)) on the Y-axis. The capacitive behaviour of the electrode-aqueous system can be reflected at the low frequency region (0.1-100 Hz) where the relationship between Z and frequency becomes linear with a slope of −1 and the phase angle reaches a maximum within this region. At the high frequency region (100-10000 Hz), the Z values are low and relatively constant, while the phase angle decreases towards zero. This is a typical response of a resistor to the AC with high frequency, corresponding to solution resistance.

A series of blank experiments were performed in order to determine the effect of cathodic scans on EIS. The pyrite electrode pretreated in the background solution at negative potentials down to −0.6 V had little influence on the EIS spectra. The experimental data were fitted well with the proposed equivalent electrical circuit shown in Fig. 3 using computer program Zview. The extracted model parameters from the equivalent circuit are given in Table 1. Compared with the untreated pyrite electrode, pretreating the pyrite electrode in the copper cyanide solution with

CN/Cu=2/1 at all polarization potentials leads to the increased values of Y_0, which is consistent with the decrease of impedance values at the low frequency region (Fig. 4(a)). This is due to the formation of Cu(I)-sulfide with high capacitance (Stevic and Rajcic-Vujasinovic, 2006) on pyrite surfaces. It is in line with the increased permittivity on sphalerite surfaces upon reacting with Cu^{2+} (Bessiere et al., 1986; Bessiere et al., 1990).

The amount of copper on pyrite surfaces can be calculated from the integrated charge over the area of Cu_2S/CuS oxidation at A3 in the voltammograms shown in Fig. 1(b). As the true area of the polished electrode is normally twice of its geometric area (Chen, 1998), the copper mass density on pyrite polarized at −0.6 V is calculated as 0.09 mg cm^{-2} (x=1 in Equation (7)). It has been reported that a monolayer of Cu on a (110) surface of pyrite is 0.07 mg cm^{-2} (Tao et al., 1994). Thus, the formed copper species on pyrite polarized at −0.6 V is approximately one molecular layer. In this study, the EIS models were, therefore, established on a basis of monolayer adsorption. In fact, the system reached an equilibrium after 2 min of pretreatment in the copper cyanide solution with no further change of current density at A3 or C3 on the voltammograms in Fig. 1(b) and no further change of the capacitance values in Table 1.

Equation (10) suggests that an increase in the surface coverage of Cu(I)-sulfides would increase the effective area of the capacitor, leading to an increase in capacitance. Therefore, the larger Y_0 values in Table 1 confirm the greater copper uptake on pyrite surfaces polarized at more negative potentials. Compared to the untreated pyrite, there is a slight increase in charge transfer resistance (R_{ct}) and decrease in electrical double layer capacitance (C_{dl}) when the pyrite was treated in the copper cyanide solution, indicating the modification of pyrite surfaces by copper species and the inhibited electrochemical redox processes of pyrite. R_{ct} values increase and C_{dl} values decrease with increasing the polarization potential, which suggests the inhibited copper

uptake. The passivation of pyrite surface reactivity by Cu(I)-sulfides is consistent with the observation in voltammetry studies.

3.2. The Effect of CN/Cu Ratios on Copper Adsorption on Pyrite Surfaces

The voltammograms of the pyrite electrode pretreated in copper cyanide solutions with the CN/Cu ratio being 2/1, 2.5/1, 3/1, 3.5/1 and 4/1 is shown in Fig. 5. The polarization potential was set at −0.6 V to achieve the maximum copper adsorption. A decrease in current density at A3 and C3 was observed with increasing the CN/Cu ratio, indicating a reduced amount of Cu_2S formed on pyrite surfaces. Peaks at A3 and C3 almost disappeared at CN/Cu=4/1. However, peaks A1, A2, C1 and C2 corresponding to the oxidation and reduction of pyrite itself, respectively, are still strongly inhibited at CN/Cu=4/1.

Bode plots for the pyrite electrode polarized at −0.6 V in copper cyanide solutions with various CN/Cu ratios is illustrated in Fig. 6. The experimental data were fitted with the proposed equivalent electrical circuit shown in Fig. 3 using computer program Zview, and the extracted model parameters from the equivalent circuit are given in Table 2. The decreases of Y_0 and C_{dl} and the increase of R_{ct} were observed with increasing the CN/Cu ratio, which is consistent with the observation from the voltammograms. EIS studies confirm the inhibition of Cu(I)-sulfide formation on pyrite surfaces at high CN/Cu ratios.

4. Discussion

This study reveals that reactions involving copper species take place on pyrite surfaces in copper cyanide solutions. The reaction products formed and their concentrations on pyrite surfaces vary with both the polarization potential and the CN/Cu ratio in solution. The mechanisms underpinning these observations may be related to copper species occurring in

copper cyanide solutions, their coordination with pyrite and the nature of the dissolution of reaction products by cyanide-bearing species which are discussed below.

4.1. Copper Cyanide Speciation

In copper cyanide solutions, the following reactions may occur:

$$CuCN \leftrightarrow Cu^{+} + CN^{-} \quad (12)$$

$$Cu(CN)_2^{-} \leftrightarrow Cu^{+} + 2CN^{-} \quad (13)$$

$$Cu(CN)_3^{2-} \leftrightarrow Cu^{+} + 3CN^{-} \quad (14)$$

$$Cu(CN)_4^{3-} \leftrightarrow Cu^{+} + 4CN^{-} \quad (15)$$

$$HCN \leftrightarrow CN^{-} + H^{+} \quad (16)$$

In the present study, the copper cyanide speciation under the experimental conditions was modelled using a computer program Visual MINTEQ (version 3.0), and the solubility product constants and reaction equilibrium constants were also obtained from this program (Gustafsson 2012). In this modelling, copper(I) cyanide was specified as a finite solid phase and was dissolved by NaCN at 25°C. The solubility product (K_{sp}) of CuCN was $10^{-19.5}$. The corresponding equilibrium constants for Equations (13) to (15) were $10^{-23.9}$, $10^{-29.2}$, $10^{-30.7}$, respectively. The *pK*a of HCN was 9.21. Parameters such as redox potential (*Eh*), pH and the molality of CuCN, CN^{-} and the balanced Na^{+} were considered to formulate the input data for the calculation. Cu^{+}/Cu^{2+} redox couple was specified with log*K*=2.69. The *Eh* ranging from −0.4 V to 0.4 V (SHE) has little influence on the activity of Cu^{+} and all cyanide-bearing species at CN/Cu ≥ 2.5/1. However, the system at CN/Cu=2/1 is unstable and easily oxidized to cupric species in contact with air according to Equation (17) (Casella and Gatta, 2000).

$$Cu(CN)_2^{-} + 0.25O_2 + 0.5H_2O + OH^{-} \rightarrow Cu(OH)_2 + 2CN^{-} \quad (17)$$

Thus all the copper cyanide solutions were prepared under the protection of nitrogen gas in this study. The speciation results are shown in Table 3. Note that the dissolution of CuCN by NaCN is incomplete at CN/Cu=2/1 and the concentration of undissolved CuCN is 1.42×10^{-5} M. Table 3 indicates that the concentrations of copper and cyanide species in coper cyanide solutions vary with the CN/Cu ratio. With increasing the CN/Cu ratio, the concentration of cyanide (CN^- and HCN) increases, while the concentration of copper ions (Cu^+ and Cu^{2+}) and copper cyanide complexes ($Cu(CN)_2^-$, $Cu(CN)_3^{2-}$, $Cu(CN)_4^{3-}$) decreases. These species and their concentrations may affect the copper coordination with pyrite and the dissolution of Cu(I)-Sulfides from pyrite surfaces.

4.2. Copper Coordination with Pyrite

The present results show that the copper in copper cyanide solutions can be coordinated to sulfur sites on pyrite with the formation of Cu(I)-sulfides at a low CN/Cu ratio. Table 3 shows that $Cu(CN)_2^-$ is the predominant species in the copper cyanide solution with CN/Cu=2/1, where the adsorption of copper on pyrite is of most significance. If a simple coordination is considered, the dissolution of $Cu(CN)_2^-$ to make Cu^+ available in contact with pyrite can be the rate-determining process. At around the open circuit potential of pyrite, S dimers predominantly exist on pyrite surfaces, although a small fraction of S monomers may co-exists (Von Oertzen et al., 2007). This study suggests that S dimers can accommodate Cu^+ with the formation of Cu(I)-S on the surface and the interaction between $Cu(CN)_2^-$ and pyrite is then suggested in Equation (18).

$$6Cu(CN)_2^- + 3FeS_2 \rightarrow 6CuS + 2Fe(CN)_6^{4-} + Fe^{2+} \qquad (18)$$

At more negative potentials, the reduction of S dimers to S monomers will occur and the pyrite surface can be reconstructed with properties resembling those of pyrrhotite (FeS). The formation of FeS is shown in Equation (5) or Equation (6). This study suggests that S monomers in the

structure of FeS are able to accommodate Cu^+ with the formation of $Cu(I)_2$-S on the surface and the reaction is suggested in Equation (19).

$$6Cu(CN)_2^- + 3FeS \rightarrow 3Cu_2S + 2Fe(CN)_6^{4-} + Fe^{2+} \quad (19)$$

The standard free energies of formation for the corresponding Fe-Cu-S-CN species are shown in Table 4. The negative changes in Gibbs free energies of Equations (18) and (19) support that the reaction processes would be thermodynamically possible. Water soluble HS^- and H_2S generated from the cathodic decomposition of pyrite or polysulfide rapidly escapes from the surface upon stirring and, thus, its contribution to copper sulfide formation on electrode surfaces should be negligible in the present experiments.

The activation energy of copper adsorption on pyrite surfaces is determined by the solubility of these Cu(I)-sulfides and the distribution of the corresponding metal ions in solution. The dissolution of Cu_2S and CuS takes place through Equations (20) and (21), respectively.

$$Cu_2S \rightarrow 2Cu^+ + S^{2-} \quad (20)$$

$$CuS \rightarrow Cu^{2+} + S^{2-} \quad (21)$$

The K_{sp} for Cu_2S dissolution is $10^{-34.92}$ in Equation (20) (Gustafsson, 2012). Assuming that the S monomer activity in FeS-like surfaces is the same as its mole fraction, the equilibrium Cu^+ activity in Equation (20) is then calculated to be 5.01×10^{-18}. As shown in Table 3, the Cu^+ activity at CN/Cu<4/1 is sufficient to maintain the growth of Cu_2S on FeS-like pyrite surfaces. On the other hand, the dissolution of CuS is a redox reaction, releasing Cu^{2+} and S^{2-} in the solution although CuS consists of Cu(I) and S dimers (Goh et al., 2006). The K_{sp} of CuS dissolution is $10^{-22.22}$ in Equation (21) (Gustafsson, 2012). Assuming the same S activity as that in Equation (20), the equilibrium Cu^{2+} activity in Equation (21) is 1.09×10^{-22}. The thermodynamic calculation shows that the Cu^{2+} activity decreases with decreasing the redox

potential. For the present deoxygenated system, at the polarization potential=0 V and CN/Cu>2/1, the Cu^{2+} activity shown in Table 3 is insufficient to maintain the growth of CuS. This can interpret the lower copper uptake efficiency on pyrite surfaces at 0 V and −0.2 V when CuS is the predominant reaction product. In fact, it has been reported that S monomers are more effective sites than S dimers for copper coordination and all S monomers but only some S dimers on a surface react with the adsorbed Cu atoms (Von Oertzen et al., 2007).

It is known that the surface of sulfides are heterogeneous in nature with regard to the distribution of binding sites. In this study, the inactive sites are due to either the hydroxide coating or the competitive adsorption of cyanide. Therefore, the lower adsorption efficiency of copper on pyrite surfaces at high polarization potentials could also be due to the limited number of active sites on pyrite surfaces to coordinate with the adsorbate. When reduction processes occur below −0.4 V, some of the inactive sites become active due to the removal of insoluble ferric hydroxides.

4.3. Dissolution of Cu(I)-Sulfides by Cyanide-Bearing Species

Table 3 shows that the concentration of Cu^{2+} in solution decreases quickly when the CN/Cu ratio increases above 2.5/1, accelerating the dissolution of CuS formed at more positive potentials. The voltammograms in Fig. 5 and the EIS in Fig. 6 show a strong CN/Cu ratio dependence of Cu_2S formation on pyrite surfaces. The concentration of both $Cu(CN)_2^-$ and Cu^+ in solution decrease when the CN/Cu ratio increases from 2/1 to 4/1, leading to a less amount of Cu_2S formed on pyrite surfaces. The copper adsorption at −0.6 V corresponding to Cu_2S formation is negligible with CN/Cu=4/1.

The effect of CN/Cu ratios on copper adsorption is due to the dissolution of Cu(I)-sulfides by cyanide-bearing species in solution. As seen in Table 3, the concentration of $Cu(CN)_3^{2-}$ becomes

higher with increasing the CN/Cu ratio from 2/1 to 4/1. The dissolution of Cu(I)-sulfides by $Cu(CN)_3^{2-}$ has been observed in cyanide leaching processes through Equation (22) (Breuer et al., 2005).

$$Cu_2S + 4Cu(CN)_3^{2-} = 6Cu(CN)_2^{-} + S^{2-} \quad (22)$$

The cyanide bearing species CN^-, HCN, and $Cu(CN)_4^{3-}$ are all able to dissolve Cu(I)-sulfides in a more efficient way than $Cu(CN)_3^{2-}$. In fact, the concentration of these cyanide-bearing species becomes higher with increasing the CN/Cu ratio as shown in Table 3, indicating the higher dissolution rate of Cu(I)-sulfides. The untreated pyrite surface actually exhibits a high reactivity as can be seen from its low charge transfer resistance R_{ct} as shown in Table 1 and there is a double layer formed as a result of the interaction with solution species. The presence of these cyanide-bearing species not only dissolves surface copper species, but also strongly inhibits the surface reactivity of pyrite. This can be seen from the increased R_{ct} and decreased C_{dl} with increasing the CN/Cu ratio as shown in Table 2, as well as the low current density of pyrite oxidation at A1 and A2 and reduction at C1 and C2 as shown on voltammograms in Fig. 5.

Therefore, the adsorption of copper on pyrite surfaces from copper cyanide solutions is a result of the equilibrium between copper coordination and Cu(I)-sulfide dissolution. The coordination process surpasses the dissolution process only at a relatively low polarization potential and a relatively low CN/Cu ratio.

5. Conclusion

Copper adsorption on pyrite surfaces from copper cyanide solutions is highly dependent on the electrochemical environments including the redox potential as well as the cyanide-to-copper ratio in solution. Reducing the polarization potential from 0 V to −0.6 V significantly promotes the copper uptake at pH 7, while increasing the CN/Cu ratio from 2 to 4 inhibits the copper

uptake. The reaction products are potential dependent, with covellite-like sulfide formed at more positive potentials and chalcocite-like sulfide formed at more negative potentials. Both of these Cu(I)-sulfides form a sub monolayer on pyrite surfaces. A simple coordination model between copper-bearing species, $Cu(CN)_2^-$, and S dimers at more positive potentials or S monomers at more negative potentials interprets the process of incorporation of Cu^+ in pyrite. In addition, the dissolution of Cu(I)-sulfides by cyanide-bearing species occurs, especially at a higher CN/Cu ratio, compromising the total copper uptake.

Acknowledgment

The authors acknowledge the financial support of this study from Newcrest and Morobe Joint Venture with the grant number of UQ2012002828. The first author also thanks the scholarship provided by the University of Queensland. This work was performed in part at the Queensland node of the Australian National Fabrication Facility.

References

Adams, M. D; Impact of Recycling Cyanide and its Reaction Products on Upstream Unit Operations. *Miner. Eng.* **2013**, *53*, 241-255.

Beltramo G.L.; Shubina T.E.; Mitchell S.J.; Koper M.T.M. Cyanide Adsorption on Gold Electrodes: A Combined Surface Enhanced Raman Spectroscopy and Density Functional Theory Study, *J. Electroanal. Chem.* **2004**, *563*, 111-120.

Bessiere, J.; Chlihp, K.; Thiebaut, J. M. Utilisation des Techniques Dielectriques Pour l'etude in situ de l'activation de la Sphalerite par les ions Cu^{2+}. *Electrochim. Acta* **1986**, *3*, 63-69.

Bessiere, J.; Chlihp, K.; Thiebaut, J. M.; Roussy, G. Dielectric Study of the Activation and Deactivation of Sphalerite by Metallic Ions. *Int. J. Miner. Process.* **1990**, *28*, 1-13.

Breuer, P. L.; Dai, X.; Jeffrey, M. I. Leaching of Gold and Copper Minerals in Cyanide Deficient Copper Solutions. *Hydrometallurgy* **2005**, *78*, 156-165.

Buckley, A. N.; Woods, R. The Surface Oxidation of Pyrite. *Appl. Surf. Sci.* **1987**, *27*, 437-452.

Casella, I. G.; Gatta, M. Anodic Electrodeposition of Copper Oxide/Hydroxide Films by Alkaline Solutions containing Cuprous Cyanide Ions. *J. Electroanal. Chem.* **2000**, *494*, 12-20.

Chandra, A. P.; Gerson, A.R. A Review of the Fundamental Studies of the Copper Activation Mechanisms for Selective Flotation of the Sulfide Minerals, Sphalerite and Pyrite. *Adv. Colloid Interface Sci.* **2009**, *145*, 97-110.

Chen, Z. Electrochemical Studies of Copper-Activation of Sphalerite and Pyrite. PhD dissertation, Virginia Polytechnic Institute and State University, **1998**.

Chen Z.; Yoon R. H. Electrochemistry of Copper Activation of Sphalerite at PH 9.2, *Int. J. Miner. Process.* **2000**, *58,* 57-66.

Dai, X.; Simons, A.; Breuer P. A Review of Copper Cyanide Recovery Technologies for the Cyanidation of Copper containing Gold Ores. *Miner. Eng.* **2012**, *25*, 1-13.

Elgillani, D. A.; Fuerstenau M. C. Mechanisms involved in Cyanide Depression of Pyrite, *Transactions AIME (Society of Mining Engineers)* **1968**, *241*, 437-445.

Finkelstein, N. P. The Activation of Sulphide Minerals for Flotation: A Review. *Int. J. Miner. Process.* **1997**, *52*, 81-120.

Fornasiero, D., Ralston, J. Iron hydroxide complexes and their influence on the interaction between ethyl xanthate and pyrite, *J. Colloid Interface Sci.* **1992**, 151, 225–235.

Fuerstenau M. C.; Jameson G. J.; Yoon R.-H. Froth flotation: A century of innovation: Society for Mining, Metallurgy, and Exploration **2007**, Littleton, Colorado.

Goh S.W.; Buckley A. N.; Lamb R. N. Copper(II) sulfide? , *Miner. Eng.* **2006**, *19*, 204-208.

Guo B.; Peng Y.; Espinosa-Gomez R. Effects of Free Cyanide and Cuprous Cyanide on the Flotation of Gold and Silver Bearing Pyrite, *Miner. Eng.* **2015**, *71*, 194-204.

Gustafsson J.P.; Visual MINTEQ, version 3.0. Compiled in Visual Basic NET2005, KTH, Department of Land and Water Resources Engineering, Stockholm, Sweden, **2012**.

Hamilton, I. C.; Woods, R. An Investigation of Surface Oxidation of Pyrite and Pyrrhotite by Linear Potential Sweep Voltammetry. *J. Electroanal. Chem.* **1981**, *118*, 327-343.

Hepler L. G.; Sweet J. R.; Jesser R. A. Thermodynamics of Aqueous Ferricyanide, Ferrocyanide and Cobalticyanide Ions, *J. Am. Chem. Soc.* **1960**, 82(2), 304-306.

Hope G.; Buckley F.M.; Munce C.G.; Woods R. Gold Enhanced Spectroelectrochemical Investigation of 2-Mercaptobenzothiazole, Isopropyl Xanthate and Butylethoxycarbonylthiourea Adsorption on Minerals, *Miner. Eng.* **2007**, *20*, 964-969.

Hope G.A.; Woods R.; Munce C.G. Raman Microprobe Mineral Identification, *Miner. Eng.* **2001**, *14*, 1565-1577.

Ishii M.; Shibata K.; Nozaki H. Anion Distributions and Phase Transitions in $CuS_{1-x}Se_x$(x = 0-1) Studied by Raman Spectroscopy, *J. Solid. State. Chem.* **1993**, *105*, 504-511.

Janetski, N. D.; Woodburn, S. I.; Woods R. An Electrochemical Investigation of Pyrite Flotation and Depression, *Int. J. Miner. Process.* **1977**, *4*, 227-239.

Jiang C. L.; Wang X. H.; Parekh B. K.; Leonard J. W. The surface and solution chemistry of pyrite flotation with xanthate in the presence of iron ions, *Colloid. Surface. A* **1998**, *136*, 51-62.

Laajalehto, K.; Leppinen, J.; Kartio, I.; Laiho, T. XPS and FTIR Study of the Influence of Electrode Potential on Activation of Pyrite by Copper or Lead. *Colloid Surface A* **1999**,*154*, 193-199.

Leppinen, J. O. FTIR and Flotation Investigation of the Adsorption of Ethyl Xanthate on Activated and Non-activated Sulfide Minerals. *Int. J. Miner. Process.* **1990**, *30*, 245-263.

Lopez-Valdivieso A.; Sanchez A. L.; Song S. On the Cathodic Reaction Coupled with the Oxidation of Xanthates at the Pyrite/Aqueous Solution Interface, *Int. J. Miner. Process.* **2005**, *77*, 154-164.

Lotter N. Cyanide volatilisation from gold leaching operations and tailing storage facilities, Dissertation, University of Pretoria, 2006.

Lu, J. M.; Dreisinger, D. B.; Cooper, W. C. Thermodynamics of the Aqueous Copper-Cyanide System. *Hydrometallurgy* **2002**, *66*, 23-36.

Lukey, G. C.; Van Deventer, J. S. J.; Huntington, S. T.; Chowdhury, R. L.; Shallcross, D. C. Raman Study on the Speciation of Copper Cyanide Complexes in Highly Saline Solutions. *Hydrometallurgy* **1999**, *53*, 233-244.

Mernagh T.P.; Trudu A.G. A laser Raman Microprobe Study of Some Geologically Important Sulphide Minerals, *Chem. Geol.* **1993**, *103*, 113-127.

Murphy R.; Strongin D. R. Surface Reactivity of Pyrite and Related Sulphides, Surf. Sci. Rep. **2009**, *64*, 145.

Parker G.; Woods R.; Hope G. Raman Investigation of Sulfide Leaching, *Electrochemical Society Proceedings*, **2003**, *18*, 181-192.

Peng Y, Grano S, Fornasiero D, Ralston J, Control of Grinding Conditions in the Flotation of Chalcopyrite and its Separation from Pyrite, *Int. J. Miner. Process.* **2003**, *69*, 87-100.

Pettinger B.; Picardi G.; Schuster R.; Ertl G. Surface-Enhanced and STM Tip-Enhanced Raman Spectroscopy of CN Ions at Gold Surfaces, *J. Electroanal. Chem.* **2003**, *554/555*, 293-299.

Prestidge, C. A.; Skinner, W. M.; Ralston, J.; Smart, R. S. C. Copper(II) Activation and Cyanide Deactivation of Zinc Sulphide under Mildly Alkaline Conditions. *Appl. Surf. Sci.* **1997**, *108*, 333-344.

Seke, M. D.; Pistorius, P. C. Effect of Cuprous Cyanide, Dry and Wet Milling on the Selective Flotation of Galena and Sphalerite. *Miner. Eng.* **2006**, *19*, 1-11.

Stevic, Z.; Rajcic-Vujasinovic, M. Chalcocite as a Potential Material for Supercapacitors. *J. Power. Sources.* **2006**, *160*, 1511-1517.

Tao D. P.; Li Y. Q.; Richardson P. E.; Yoon R. H. The Incipient Oxidation of Pyrite, *Colloids and Surfaces A.* **1994**, 93, 229- 239.

Tovlmix P.; Brtok P. B. A Thermodynamic Study of Pyrite and Pyrrhotite, *Geochim. Cosmochim. Ac*. **1964**, 78, 641-671.

Tao, D. P.; Richardson, P. E.; Luttrell, G. H.; Yoon, R. H. Electrochemical Studies of Pyrite Oxidation and Reduction using Freshly-Fractured Electrodes and Rotating Ring-Disc Electrodes. *Electrochim. Acta* **2003**, *48*, 3615-3623.

Turcotte S.B.; Benner R.E.; Riley A.M.; Li J.; Wadsworth M.E.; Bodily D, Application of Raman Spectroscopy to Metal-Sulfide Surface Analysis, *Appl. Opt.* **1993**, *32*, 935.

Velásquez, P.; Leinen, D.; Pascual, J.; Ramos-Barrado, J. R.; Grez, P.; Gomez, H.; Schrebler, R.; Del Río, R.; Córdova, R. A Chemical, Morphological, and Electrochemical (XPS, SEM/EDX, CV, and EIS) Analysis of Electrochemically Modified Electrode Surfaces of Natural Chalcopyrite ($CuFeS_2$) and Pyrite (FeS_2) in Alkaline Solutions. *J. Phys. Chem. B* **2005**, *109*, 4977-4988.

Velásquez, P.; Leinen, D.; Pascual, J.; Ramos-Barrado, J. R.; Cordova, R.; Gomez, H.; Schrebler, R. XPS, SEM, EDX and EIS Study of an Electrochemically Modified Electrode Surface of Natural Chalcocite (Cu_2S). *J. Electroanal. Chem.* **2001**, *510*, 20-28.

Von Oertzena G.U.; Skinner W.M.; Nesbitt H.W. Ab Initio and XPS Studies of Pyrite (1 0 0) Surface States. *Radiation Physics and Chemistry*. **2006**, *75*, 1855-1860.

Von Oertzen G.U.; Skinner W. M.; Nesbitt H. W.; Pratt A. R.; Buckley A.N. Cu Adsorption on Pyrite (100): Ab Initio and Spectroscopic Studies. *Surface Science* **2007,** *601*, 5794-5799.

Wang, X.; Forssberg, E. The Solution Electrochemistry of Sulfide-Xanthate-Cyanide Systems in Sulfide Mineral Flotation, *Miner. Eng.* **1996**, *9*, 527-546.

Wang X.; Forssberg E.; Bolin N. J. Thermodynamic Calculations on Iron-Containing Sulphide Mineral Flotation Systems, I. The Stability of Iron-Xanthates**,** *Int. J. Miner. Process.* **1989a**, *27*, 1-19.

Wang, X.; Forssberg, E.; Bolin N. J. The Aqueous and Surface Chemistry of Activation in the Flotation of Sulphide Minerals-A Review. Part I: An Electrochemical Model. *Miner. Process. Extr. Metall. Rev.* **1989b**, *4*, 135-165.

Weisener, C.; Gerson, A. An Investigation of the Cu (II) Adsorption Mechanism on Pyrite by ARXPS and SIMS. *Miner. Eng.* **2000a**, *13*, 1329-1340.

Weisener, C.; Gerson, A. Cu(II) Adsorption Mechanism on Pyrite: an XAFS and XPS Study, *Surf. Interface Anal.* **2000b**, *30*, 454-458.

Woods R.; Yoon R.H.; Young C.A. Eh-pH Diagrams for Stable and Metastable Phases in The Copper-Sulfur-Water System, *Int. J. Miner. Process.* **1987**, *20*, 109-120.

Yoon, R. H.; Lagno, M. L.; Latrell, G. H.; Mielczark, A. In Processing and Utilization of High Sulfur Coals IV; Dugau PR, Quigley DR, Attia YA, Eds.; Elsevier: Amsterdam, **1991**, p 291.

Figure captions

Fig. 1. The voltammogram of the untreated pyrite electrode (a), and the pyrite electrode pretreated in the copper cyanide solution with CN/Cu=2/1 at 0 V, −0.2 V, −0.4 V and −0.6 V (b): background solution of 0.1 M KH_2PO_4; pH 7; a scan rate of 0.02 V s^{-1}.

Fig. 2. Raman spectra of the untreated pyrite electrode and the pyrite electrode pretreated in the copper cyanide solution with CN/Cu=2/1 at 0 V, −0.2 V, −0.4 V, and −0.6 V.

Fig. 3. The electrical circuit that models the impedance spectra.

Fig. 4. Bode plots (EIS) of the untreated pyrite electrode and the pyrite electrode pretreated in the copper cyanide solution with CN/Cu=2/1 at 0 V, −0.2 V, −0.4 V, and −0.6 V with the background solution of 0.1 M KH_2PO_4 at pH 7: (a) impedance with frequency; (b) phase angle with frequency.

Fig. 5. The voltammograms of the pyrite electrode pretreated in copper cyanide solutions with the CN/Cu ratio being 2/1, 2.5/1, 3/1, 3.5/1 and 4/1 at −0.6 V: background solution of 0.1 M KH_2PO_4; pH 7; a scan rate of 0.02 V s^{-1}.

Fig. 6. Bode plots (EIS) of the untreated pyrite electrode and the pyrite electrode pretreated in copper cyanide solutions with CN/Cu=2/1, 2.5/1, 3/1, 3.5/1, or 4/1 at −0.6 V with the background solution of 0.1 M KH_2PO_4 at pH 7: (a) impedance with frequency; (b) phase angle with frequency.

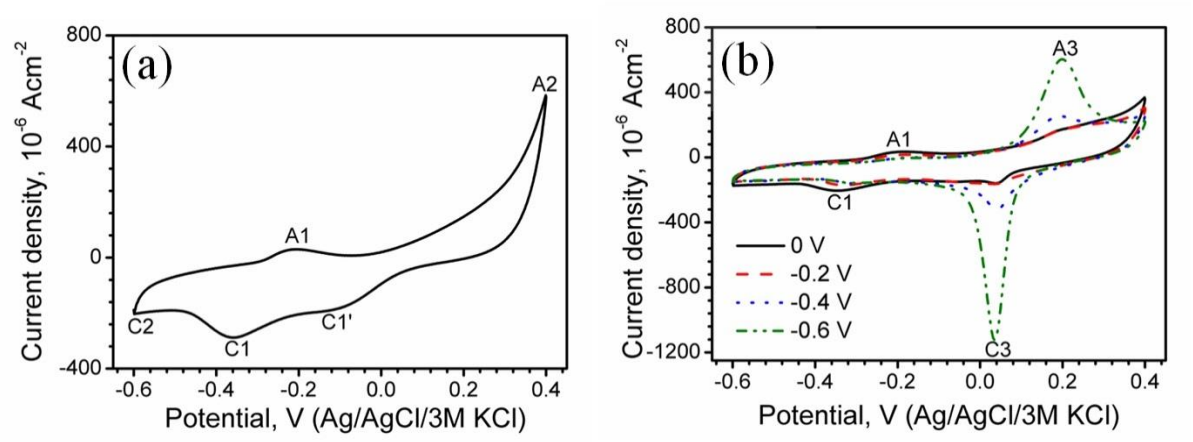

Fig. 1.

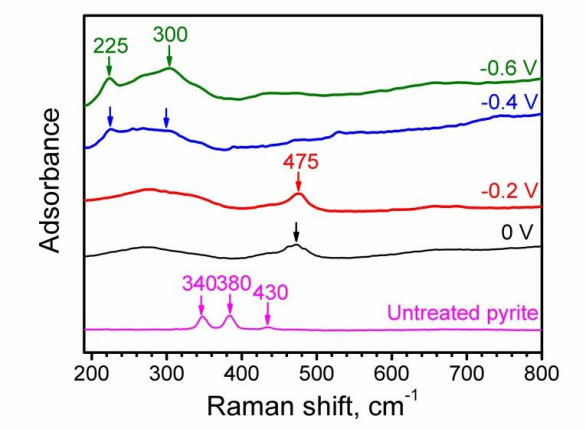

Fig. 2.

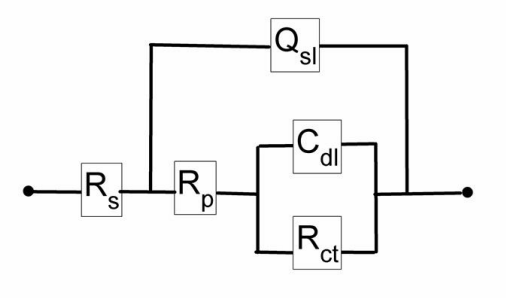

Fig. 3.

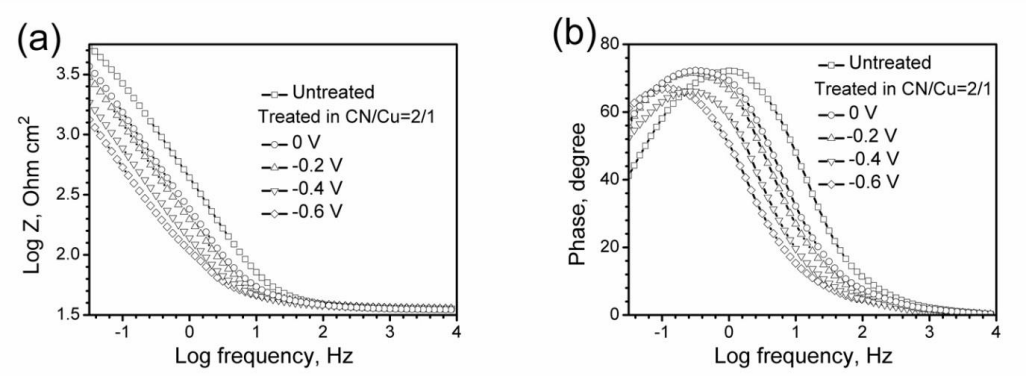

Fig. 4.

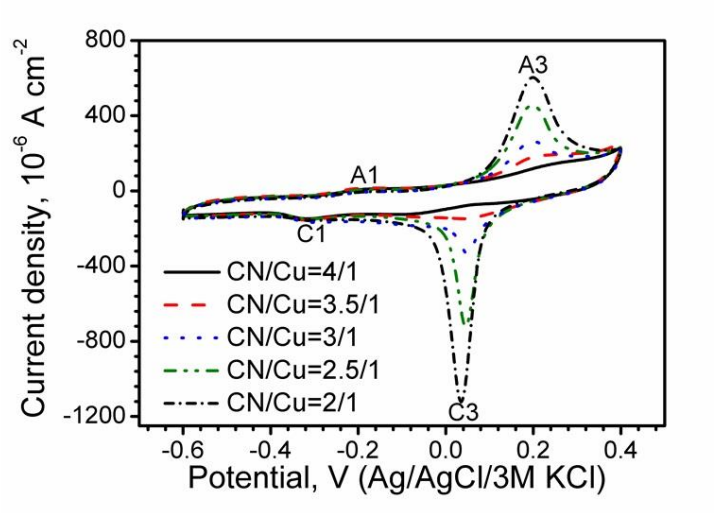

Fig. 5.

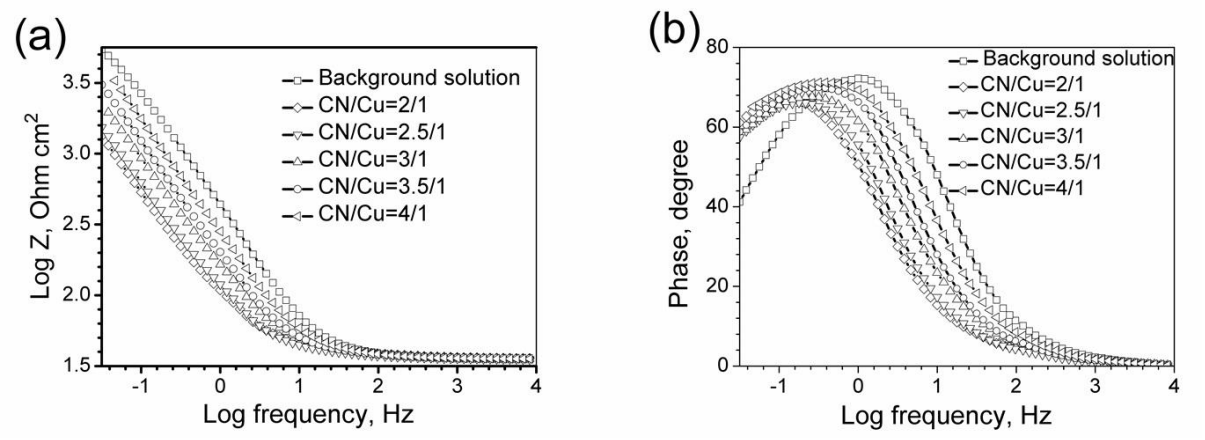

Fig. 6.

Table captions

Table 1 Parameters of the equivalent circuit simulated from EIS for the untreated pyrite electrode and the pyrite electrode pretreated in the copper cyanide solution with CN/Cu=2/1 at various potentials.

Table 2 Parameters of the equivalent circuit simulated from EIS for the pyrite electrode pretreated in copper cyanide solutions with various CN/Cu ratios at -0.6 V.

Table 3 The activity of copper and cyanide species in copper cyanide solutions with various CN/Cu ratios.

Table 4 Fe-Cu-S-CN species and their standard free energies of formation.

Table 1

	Untreated pyrite	−0.6	−0.4	−0.2	0
$R_s(\Omega \cdot cm^2)$	36.2	36.6	36.9	35.9	35.1
$C_{dl}(10^{-5}F/cm^2)$	96.5	52.6	46.8	26.0	17.2
$R_{ct}(k\Omega \cdot cm^2)$	2.5	8.35	8.68	8.8	11.5
$Y_0(10^{-5}S \cdot s^n/cm^2)$	52.3	215.7	182	115.9	76.2
n	0.88	0.76	0.82	0.84	0.81
$R_p(\Omega \cdot cm^2)$	2710	59.9	40.8	41	37.3

Table 2

	CN/Cu			
	2.5	3	3.5	4
$R_s(\Omega \cdot cm^2)$	35.5	34.2	35.8	35.4
$C_{dl}(10^{-5}F/cm^2)$	36.0	26.8	17.5	10.1
$R_{ct}(k\Omega \cdot cm^2)$	6.47	10.1	11.3	19.1
$Y_0(10^{-5}S \cdot s^n/cm^2)$	192.6	130.6	98.2	71.1
n	0.77	0.77	0.80	0.81
$R_p(\Omega \cdot cm^2)$	41	48.5	34.5	38.5

Table 3

	CN to Cu ratio				
Species	2	2.5	3	3.5	4
CN^-	3.75×10^{-8}	1.50×10^{-6}	3.41×10^{-6}	5.68×10^{-6}	8.19×10^{-6}
$Cu(CN)_2^-$	9.43×10^{-4}	7.11×10^{-4}	5.29×10^{-4}	4.03×10^{-4}	3.18×10^{-4}
$Cu(CN)_3^{2-}$	7.06×10^{-6}	2.13×10^{-4}	3.60×10^{-4}	4.57×10^{-4}	5.20×10^{-4}
$Cu(CN)_4^{3-}$	8.39×10^{-12}	1.01×10^{-8}	3.89×10^{-8}	8.21×10^{-7}	1.35×10^{-6}
HCN (aq)	6.08×10^{-6}	2.43×10^{-4}	5.53×10^{-4}	9.21×10^{-4}	1.32×10^{-3}
Cu^+	8.42×10^{-13}	3.98×10^{-16}	5.71×10^{-17}	1.57×10^{-17}	4.95×10^{-18}
Cu^{2+}	6.10×10^{-19}	3.31×10^{-22}	4.80×10^{-23}	1.35×10^{-23}	5.06×10^{-24}

* pH=7; Eh=0 V; 25°C; Initial [CuCN]=1×10^{-3} M

Table 4

	ΔG^0_{298} kJ mol^{-1}	Ref.
$Cu(CN)_2^-$	258	(Lu et al., 2002)
$Cu(CN)_3^{2-}$	400	(Lu et al., 2002)
Cu_2S	−86.19	(Woods et al., 1987)
CuS	−53.56	(Woods et al., 1987)
Cu^+	50	(Woods et al., 1987)
Cu^{2+}	65.52	(Woods et al., 1987)
FeS_2	−166.94	(Tovlmix and Brtok, 1964)
FeS	−100.42	(Tovlmix and Brtok, 1964)
Fe^{2+}	−78.87	(Tovlmix and Brtok, 1964)
$Fe(CN)_6^{4-}$	694.92	(Hepler et al., 1960)

Highlights

- CuS forms on pyrite from copper cyanide solutions at more oxidizing potentials.
- Cu_2S forms on pyrite from copper cyanide solutions at more reducing potentials.
- The copper uptake on pyrite increases at more reducing potentials.
- Cu(I)-sulfides on pyrite are dissolved by cyanide species at high CN/Cu ratios.